Measurement 151 (2020) 107211

Contents lists available at ScienceDirect

Measurement

journal homepage: www.elsevier.com/locate/measurement

Dynamic measurement of stay-cable force using digital image techniques

Wenkang Du, Dong Lei *, Pengxiang Bai, Feipeng Zhu, Zhentian Huang

College of Mechanics and Materials, Hohai University, Nanjing 211100, PR China

ARTICLE INFO

Article history:
Received 10 August 2019
Received in revised form 29 September 2019
Accepted 27 October 2019
Available online 4 November 2019

Keywords:
Digital image processing
Digital image correlation
Cable force
Stay cable bridge
Bridge monitoring

ABSTRACT

Conventional sensors, such as the accelerometers and velocimeters, are commonly applied to estimate the vibration of stay cables for the recognition of dynamic response. Such practice is relatively time-consuming and expensive due to the challenge from considerable amount of cabling work and installation of data acquisition logger. Two measurement methods based on digital image techniques, digital image processing (DIP) and digital image correlation (DIC), are adopted in this study to identify the cable force with capturing single and multiple points images by camera. To verify the reliability of the methods, the results are compared with accelerometer, and the relative deviations between the two methods and the accelerometers are within 5%. The multi-point vibration mode of stay cable using the digital image techniques was compared to numerical simulation for exploring the role of mode difference in cable force measurement. Experimental results show that the application of the digital image techniques in stay cable bridge is sustainable and advantageous and the differences between various digital image techniques are shown clearly.

1. Introduction

With the rapid development of technology and economy, bridges have been important parts of modern transportation around the world. Due to large traffic volumes and extremely complex environments, the situation of many bridge structures is not optimistic. Thus, it is vital to develop the structure health monitoring (SHM) for the bridges. As a critical load-carrying member, cable plays a vital role in the overall safety of bridge system, therefore the tension of the cable estimated according to its dynamic properties needs to be focused on. To estimate the tension of the cable, which is continuously affected by environmental factor and traffic use, the dynamic properties should be identified.

At present, the cable force could be estimated by pressure sensor, pressure oil meter, magnetic flux and vibration method [1–4]. The pressure sensor and the pressure oil meter method, which belong to the direct method, are generally applied to the cable force measurement during bridge construction. Magnetic flux is suitable for long-term monitoring and non-contact measurement, whereas the initial cost is large and the installation convenience needs to be improved. Vibration method is extensively used in bridge structure monitoring with capturing the dynamic response by installing acceleration sensors. This means that too many cabling works need to be done to realize the requirement of data transmission. The maintenance and management of sensor are also faced with much trouble.

In order to resolve above problems, digital image techniques come into the engineering structure monitoring [5–7] and material detection and have been widely developed [8,9]. Chang and Ji [10] studied cable vibration by using non-target video measurement technology. By Canny edge detection image processing and dimensionless length matching, the cable vibration frequency and amplitude could be well obtained in the case of uncalibrated target. Based on digital image processing (DIP) technology, Lee et al. [11] used texture recognition algorithm to capture the motion of known geometry, and calculated the actual displacement of the cable through calibration. Choi et al. [12] introduced a dynamic displacement vision system, which was experienced in the masonry and two-story steel frame specimen to verify the reliability. The accuracy was improved by updating the coefficient and resizing the region of interest through this method. A set of computer software developed by Kim et al. [13,14] could be used for long-term cable force monitoring. Multiple cable forces on cable-stayed or suspension bridge could be measured simultaneously through digital image correlation (DIC) method. Tian et al. [15] presented an advanced video deflectometer using actively illuminated LED targets for bridge deflection. The video deflectometer was

* Corresponding author.
E-mail address: leidong@hhu.edu.cn (D. Lei).

https://doi.org/10.1016/j.measurement.2019.107211
0263-2241/

applied for field, remote, and multipoint deflection measurement of the Wuhan Yangtze River Bridge with strong robustness against ambient light changes. Feng et al [16] proposed a novel noncontact vision-based method for cable force measurement which was applied in structural installation stage of the Hard Rock Stadium in Florida. Satisfactory agreements were observed between measured cable forces by the vision-based sensor and the reference readings from load cells. A vision-based inspection system was also developed for detecting surface damages on cables in long-span cable-stayed bridges by Li et al. [17]. An efficient scale-invariant feature transform (SIFT) was presented to achieve the multi-image mosaic with partially overlapped regions in different defect images which were acquired by four cameras. In order to obtain more comprehensive bridge structural safety information, the digital image techniques combined with unmanned aerial vehicle UAV [18–24] and machine learning [25–31] were also widely applied to the health monitoring of bridge structures. There are many novel combinations of digital image techniques, but few studies have compared the otherness between different digital image techniques.

Different digital image techniques have their own advantages. DIC has the advantage of matching recognition accuracy and DIP has high processing efficiency. It is a crucial issue that how to evaluate the difference between the two methods. In contrast to previous studies using a single digital image method such as DIP [11–13] or DIC [9,24,32–34,41], this paper carried out a further study which combines these two methods for cable force measurement. To verify the reliability of the digital image techniques, two laboratory tests, including single point and multi-point cable force measurement, are performed and also compared with accelerometer or numerical simulation. Moreover, more exploration and thoughts are produced between different digital image techniques about diversity and application, this also provides a new thought and way for further promotion in the engineering practice. In addition, the digital image acquisition equipment employed in this paper is the ordinary Digital Single Lens Reflex (DSLR) Camera on the market, which is convenient and cheap. It can be applied not only in the long-term monitoring of stay-cable bridge, but also in the regular inspection.

2. Measurement principles

2.1. Vibration frequency method

In the vibration frequency method, the dynamic response of the stay cable is measured by a sensor. To solve the cable tensile force, the dynamic characteristics such as the vibration frequency and mode shape of the stay cable are acquired from the dynamic response. Assuming that the sag-span ratio of the cable is relatively small and the axial vibration of the cable can be ignored, the following motion equation can be concluded:

$$EI\frac{\partial^4 v(x,t)}{\partial x^4} - F\frac{\partial^2 v(x,t)}{\partial x^2} + m\frac{\partial^2 v(x,t)}{\partial x^2} = 0 \tag{1}$$

where, EI is the bending stiffness of the cable, $v(x,t)$ represents the amplitude, F is the cable force, and m is the mass of the cable per unit length. When both ends are simply supported, the boundary condition is put into:

$$\begin{cases} v(0,t) = 0 \quad v(l,t) = 0 \\ v''(0,t) = 0 \quad v''(l,t) = 0 \end{cases} \tag{2}$$

Substituting Eq. (1) into the vibration equation yields:

$$F = \frac{4ml^2 f_n^2}{n^2} - \frac{n^2\pi^2 \mathrm{EI}}{l^2} \tag{3}$$

If the bending stiffness is small, then:

$$F = \frac{4ml^2 f_n^2}{n^2} \tag{4}$$

2.2. Digital image processing

Before processing, image sampling and quantization are the first steps of image processing technology, which is the crucial part in the overall process. This process includes collecting images by acquisition equipment, image processing and converting into digital signals. Image quantization is the process of dividing the value range of each sample point into several intervals where the values of each interval could be represented by a mean value. Digital image sampling will be automatically discretized and arranged into the form of a matrix for storage. Each small area can be called a pixel and each pixel contains two attributes, namely position and gray scale.

Based on MATLAB 2017, target recognition, binarization and morphological processing, and finally obtaining the target point displacement time history diagram through dynamic capture of centroid can be realized by DIP method. A target for tracking needs to be set on the cable when measuring cable force using DIP method, and the displacement time-history diagram of cable vibration could be obtained by tracking the motion path of the target which was shown in Fig. 1(a). Therefore, it is necessary to separate the targets in the image sequence from the viewpoint background to make it stand out and reflect the vibration of the cable. In this study, false color enhancement technique, which refers to the mathematical operation of a color image, was applied to fulfill the above requirement. The general linear false color mapping can be expressed as Eq. (5). Fig. 1(b) shows the results by false color enhancement processing.

$$\begin{bmatrix} R_F \\ G_F \\ B_F \end{bmatrix} = \begin{bmatrix} a_1 & b_1 & c_1 \\ a_2 & b_2 & c_2 \\ a_3 & b_3 & c_3 \end{bmatrix} \cdot \begin{bmatrix} R_f \\ G_f \\ B_f \end{bmatrix} \tag{5}$$

Here, (R_f, G_f, B_f) represents the three primary color components of the original image and (R_F, G_F, B_F) represents that of the transformed image by false color enhancement matrix.

In order to highlight the target, eliminate useless background information and improve image processing efficiency, the binarization method is a better choice. Binary image refers to a two-dimensional array with values of 0 and 1. Each pixel is either black or white, and its gray value has no intermediate transition image. It can be seen from binary image (Fig. 1(c)) that there are still many discontinuous areas in the target, and sometimes some noises would appear around the target. Erosion and dilation are common operations in morphology. Erosion, which is a process of eliminating convenience points and shrinking the boundary points inward, can be used to eliminate small and meaningless objects while dilation is the process of merging all the background points in contact with the object into the object, making the boundary expand outward. Sometimes, it is necessary to combine the two courses for better results, which is opening and closing operation as shown in Fig. 1(d).

$$A - B = \{x, y \,|\, (B)_{xy} \subseteq A\} \tag{6}$$

$$A + B = \{x, y \,|\, (B)_{xy} \cap A \neq \varnothing\} \tag{7}$$

$$A^{\circ}B = (A - B) + B \tag{8}$$

$$A \cdot \mathrm{B} = (\mathrm{A} + \mathrm{B}) + \mathrm{B} \tag{9}$$

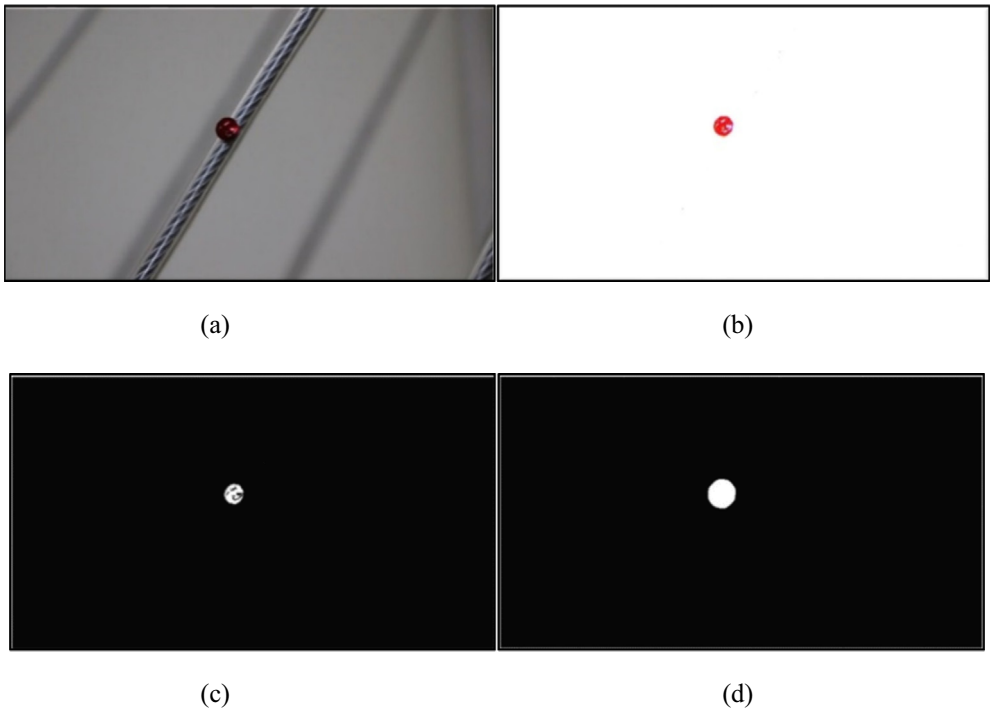

Fig. 1. (a) Original image. (b) Image with false color enhancement processing. (c) Image with binarization. (d) Image with opening and closing operation.

Eq. (6) presents the erosion and Eq. (7) presents the dilation. Eqs. (8) and (9) presents the relation between erosion and dilation in opening and closing operation, respectively. Where A is the processed region, B is the structure region.

The motion of centroid often reflects the target very well with a strong anti-noise ability. Vibration of the cable could be distinctly extracted from the dynamic response of the centroid. If the binary image with the size of the image processing region of $M \times N$ is $g(x,y)$, then the centroid coordinate of the target could be showed as Eq. (10).

$$\begin{aligned} x_c &= \sum_{x=0}^{M-1}\sum_{y=0}^{N-1} xg(x,y) / \sum_{x=0}^{M-1}\sum_{y=0}^{N-1} g(x,y) \\ y_c &= \sum_{x=0}^{M-1}\sum_{y=0}^{N-1} yg(x,y) / \sum_{x=0}^{M-1}\sum_{y=0}^{N-1} g(x,y) \end{aligned} \tag{10}$$

2.3. Digital image correlation

The DIC method has been widely developed in recent years [35,36], especially in the field of experimental mechanics [37–41]. Its principal idea is to find the maximum pertinency between the deformed image and undeformed image. The captured target patterns on cable surface before and after deformation are usually called a "reference" and a "target" image, respectively. The image matching of DIC between a reference and a target image is shown in Fig. 2(a). A circular subset from the reference image is selected and used to estimate its corresponding position in the target image. For DIC method, the region of interest and the target subregion are selected by Vic-2d software. Based on the normalized cross correlation function, the target subregions before and after deformation are matched and identified, so as to obtain the time-domain image of the cable motion and the frequency domain graph by fast Fourier transform (FFT).

Correlation function [42], which is usually used to identify the differences between two images, can be roughly classified into cross-correlation function and distance-based minimum square distance function. The cross-correlation method was selected for calculation in this paper because it can adapt to the difference between the light and lighting. Cross-correlation (CC) is a matching method which can simply determine the position of the required referenced presented target-window function in a two-dimensional interested subset. A small area centered at a certain point on the surface to be measured is selected as a subset, and the gray value feature of the rectangular area is taken as the reference. By means of CC, the dynamic feature of the target can be induced from the matching search of the neutron region of the image before and after deformation. As shown in the Fig. 2(b), the target point is shifted to (x_0', y_0') after deformation by identifying the selected subset. Within the selected subset, the adjacent point (x_i, y_i) of the target point also becomes (x_i', y_i'). The correlation of the pixel set with the subarea region in the reference image is determined by calculating the CC coefficient by

$$C(f,g) = C(x_i, y_j, x_i', y_j') = C(p) \tag{11}$$

For standard CC functions:

$$C(f,g) = \frac{\sum_{i=-M}^{M}\sum_{j=-N}^{N} f(x_i,y_j)g(x_i',y_j')}{\sqrt{\sum_{i=-M}^{M}\sum_{j=-N}^{N} f^2(x_i,y_j)}\sqrt{\sum_{i=-M}^{M}\sum_{j=-N}^{N} g^2(x_i',y_j')}} \tag{12}$$

where

$$\begin{aligned} x_i' &= x_i + u_i \\ y_j' &= y_j + v_j \end{aligned} \tag{13}$$

where, u_i and v_i represent the displacement components of any point in the x and y directions in the selected subregion. In $C(f,g)$, $f(x_i,y_j)$ and $g(x_i',y_j')$ respectively represent the grayscale distribution values before and after the deformation of the sub-region which have a gray level ranging from $-N$ to N and $-M$ to M.

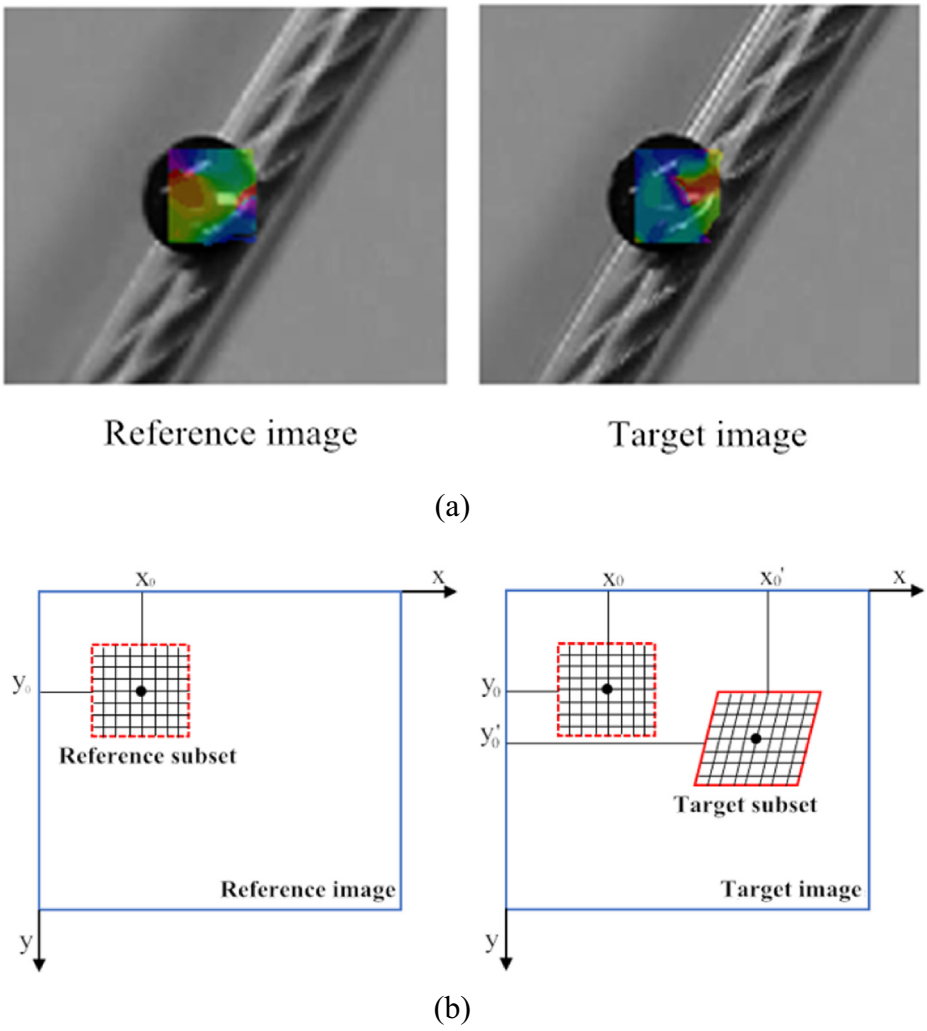

Fig. 2. (a) Subset matching of speckle images captured before and after deformation. (b) Two-dimensional digital image correlation principle.

3. Experiments and discussions of cable force measurement

3.1. Experimental instrument

The instruments used are a cable-stayed bridge model, a DSLR Camera, an acceleration sensor, lens, and a computer. The span combination of the model is 2.15 + 4.8 + 2.15 = 9.1 m and is scaled according to the scale of Guanhe Bridge (Fig. 3) at 1:70. Located at the junction of Lianyungang city and Yancheng city, Jiangsu province, Guanhe Bridge has a span of 32.9 + 115.4 + 340 + 115.4 + 32.9 = 636.6 m. A series of dynamic response experiments were conducted by a portable DSLR Camera. The acceleration sensor was also installed on the cable to measure dynamic response synchronously. The main instrument parameters are shown in Table 1.

Fig. 3. Guanhe Bridge.

3.2. Verification experiments comparing with accelerometer

To verify the digital image techniques, dynamic responses were measured in the vertical direction of the stay cable under an artificial vibration condition comparing with the accelerometer. A target and an accelerometer were installed on R03 cable to capture the dynamic response by digital image techniques and conventional method respectively as shown in Fig. 4. Before the verification, the images must be calibrated first, which means measuring the size value of each pixel. The camera was positioned perpendicular to the target plane and the focal length of the lens was

Table 1
Main instrument parameters.

Instrument	Brand	Parameter
Camera	Canon 70D	Acquisition rate: 50 frames/s Resolution: 1280×720 pixels
Lens	Canon STM	Focal length: 18–55 mm manual zoom
Acceleration Sensor	TST120A500	Sampling frequency: 100 Hz

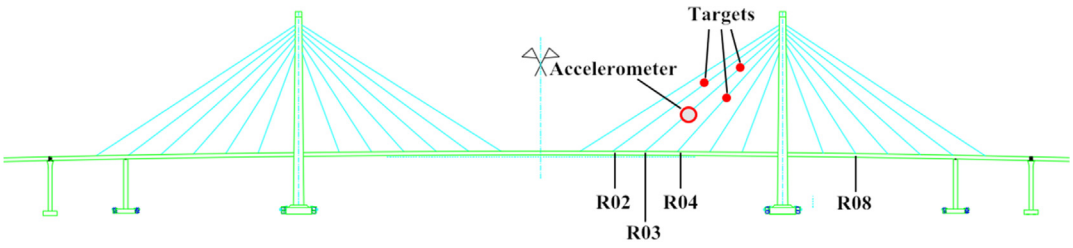

(a)

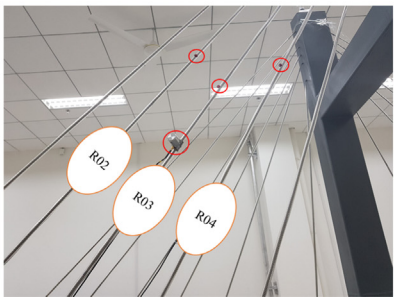

(b)

Fig. 4. The (a) diagrammatic drawing and (b) actual image of the acceleration and target placement.

adjusted to 55 mm. Meanwhile, the distance between the lens and the target was measured at 780 mm. The diameter of the target is 10 mm, and the pixel value occupied by the diameter is 63. Therefore, the unit pixel resolution is 0.159 mm. Then the camera position is fixed and artificial excitation was carried out on the cable.

Fig. 5 shows the dynamic responses and the power spectral density (PSD) function according to the FFT of stay cable R03 obtained by acceleration, DIP and DIC. To reduce the error caused by special factors, three experiments were completed to increase the reliability of the results by taking the average in this study.

Comparison results between DIP and DIC can be seen in Table 2. To validate the accuracy and precision of the estimated dynamic response, deviation analysis is performed with percent deviation shown in Eq. (14). The first-order frequency deviation of DIP is about 1.67%, and the second and the third are much smaller, respectively 1.48% and 0.47%. By contrast, the first-order deviation of DIC is relatively large, about 4.70%, and the second and third order frequency deviation are smaller, respectively 1.79% and 1.51%. Therefore, the dynamic response results concluded from the digital image techniques are found to be reliable.

$$\text{Percent deviation} = \sum_{i=1}^{n} (\delta_m - \delta_c)^2 / \sum_{i=1}^{n} (\delta_m)^2 \tag{14}$$

here, n is the number of measured data points, δ_m is the dynamic response measured by the accelerometer, and δ_c is the dynamic response estimated by the digital image techniques in Table 2. Also, δ_m represents DIP and δ_c represents DIC in Table 3 and Table 5. δ_m represents Abaqus and δ_c represents digital image method in Table 4.

3.3. Cable force measurement of single point

Fig. 6 and Fig. 7 show the PSD function for the dynamic properties of the stay cable R02 and R04 obtained by two digital image techniques. Comparing results of two methods as shown in Table 3, we can find that the first three frequencies are roughly the same with the deviation of all frequencies were within 1%, which can satisfy the actual requirements of engineering. After measurements, the length of stay cable R04 is 1.980 m and the stay cable R02 is 2.400 m. It can be found that the frequency of the stay cable R04 is slightly higher than R02, which is consistent with the analysis of vibration theory that the longer the cable is, the lower its vibration frequency is under the same condition. Nevertheless, it is interesting to note that the cable R03 is shorter than the R02, and the vibration frequency is lower. The main reason is that the mass of the sensor is larger compared with the cable, which is distinct from the relative mass on actual bridge. In other words, the measurements of cable force will be affected by sensor installation and digital image techniques have the superiority to handle these problems.

In addition, the results were also compared with the numerical simulation analysis [43] to increase their reliability for the stay cable without acceleration. The stay cable R04 was selected to simulate by Abaqus. Its material parameters include: length$l = 1.98$ m, unit length mass $= 0.1362$ kg/m, diameter of circular section $d = 6$ mm, and its elastic modulus$E = 16.3$ Gpa measured by tensile experiment. Table 4 shows a comparison between two digital image techniques and the numerical simulation of Abaqus. From the results, it can be found that the deviation of digital image techniques and numerical simulation results were less than 3% for the first three order frequencies of cable R04. Based on vibration method, the cable force of each order frequency was estimated and then average value could be obtained. The deviation of DIC method was 1.09% while the DIP method is only 0.24%, both methods show feasible results.

3.4. Cable force measurement of multi-point

Modal analysis is also an important factor in the process of cable force measurement as Fig. 10 shows. Five targets (TI-T5) were arranged on the stay cable to obtain the multi-target vibration data in this paper as shown in Fig. 8. Cable force could be concluded from the vibration frequency which is the mean value of the first three frequencies of five targets. The processing method is as

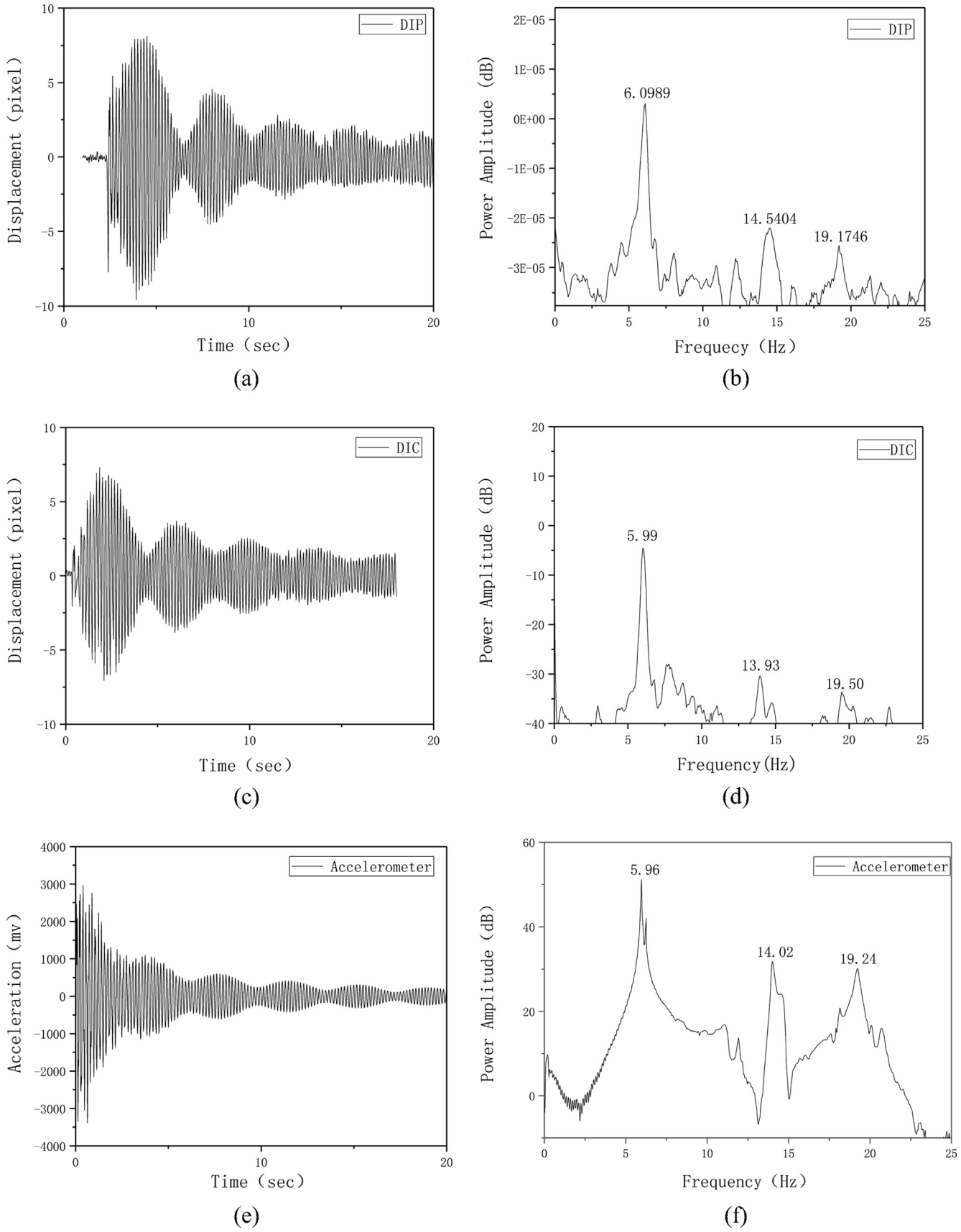

Fig. 5. Dynamic response of first vibration for stay cable R03. (a) Dynamic response and (b) PSD image of DIP. (c) Dynamic response and (d) PSD image of DIC. (e) Dynamic response and (f) PSD image of accelerometer.

Table 2
First three order frequency measurement results of stay cable R03.

Method	Number	Frequency (Hz)		
		1st	2nd	3rd
Accelerometer	1	5.95	13.98	19.01
	2	5.96	14.39	19.29
	3	5.96	13.98	19.21
	Mean value	5.96	14.12	19.17
DIP	1	5.96	13.93	19.24
	2	5.96	14.35	19.25
	3	6.25	14.70	19.30
	Mean value	6.06	14.33	19.26
	Deviation (%)	1.67	1.48	0.47
DIC	1	6.23	14.03	19.38
	2	6.25	14.02	19.51
	3	6.23	13.98	19.49
	Mean value	6.24	14.01	19.46
	Deviation (%)	4.70	0.79	1.51

Table 3
Cable force measurement results of stay cable R02 and R04 by DIC and DIP.

Cable number	Method	Frequency (Hz)			Tension (N)
		1st	2nd	3rd	
Stay cable R02 ($l_1 = 1.980$ m)	DIP	7.12	14.12	21.30	107.06
	DIC	7.07	14.18	21.25	105.89
	Deviation (%)	0.7	0.42	0.23	1.09
Stay cable R04($l_2 = 2.400$m)	DIP	6.67	13.38	20.06	140.12
	DIC	6.68	13.40	20.07	140.45
	Deviation (%)	0.15	0.15	0.05	0.24

Table 4
Cable force measurement results of stay cable R04 by digital image techniques and Abaqus.

Cable number	Method	Frequency (Hz)			Tension (N)
		1st	2nd	3rd	
Stay cable R04 ($l_1 = 1.980$ m)	Abaqus	7.03	14.21	21.83	108.82
	DIP	7.12	14.12	21.30	107.06
	Deviation (%)	1.28	0.63	2.43	1.62
	DIC	7.07	14.18	21.25	105.89
	Deviation (%)	0.59	0.21	2.66	2.69

Table 5
Cable force measurement results of five targets by DIC and DIP.

Target number	Frequency (Hz)						Tension (N)	
	1st		2nd		3rd			
	DIP	DIC	DIP	DIC	DIP	DIC	DIP	DIC
1	8.56	8.56	16.70	16.69	24.20	\	144.22	148.58
2	8.53	8.56	16.67	16.67	24.35	\	144.25	148.41
3	8.53	8.53	16.74	16.59	24.19	\	144.06	147.19
4	8.53	8.15	16.67	16.31	24.73	21.92	145.69	129.14
5	8.53	8.62	16.67	15.66	24.42	21.13	145.51	128.38
Mean value	8.54	8.48	16.69	16.38	24.39	21.53	144.75	140.34
Deviation (%)	0.70		1.86		11.73		3.05	

same as single target by DIP and DIC. Fig. 9 shows the process of two digital techniques.

Table 5 shows the comparison results of five points by two digital image techniques. The DIP maintains a satisfying stability and the first three order frequencies can be distinctly obtained. Meanwhile, the third frequency of the first three targets of digital image techniques were difficult to gain, which can only get the third order frequency of two targets. That is why the third order shows a large relative deviation of more than 10% while the first two orders have a smaller of 0.7% and 1.86%. Furthermore, the cable force corresponding to each target of five can be estimated based on the first three frequencies using two digital image techniques. After averaging, the relative deviation of stay cable force converged greatly with an acceptable range of 3.05%.

Consequently, more viable results can be obtained by solving cable force with multi-points which can also meet the actual requirements of the project. Meanwhile, the measuring errors due to more complex background changes such as bad weather,

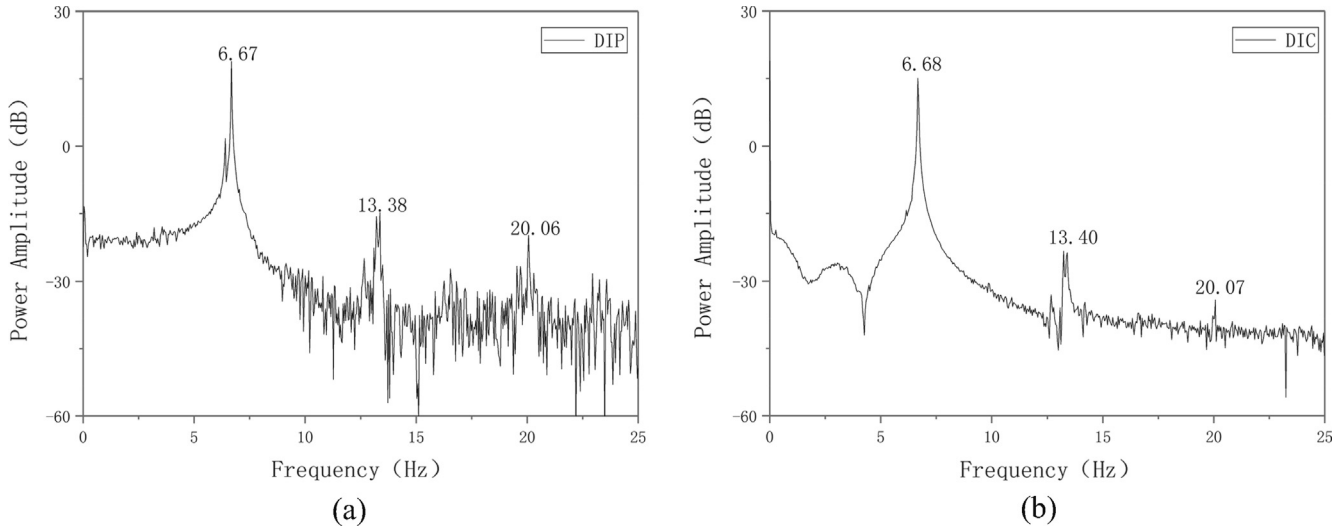

Fig. 6. (a) PSD function of stay cable R02 by digital image processing and (b) digital image correlation.

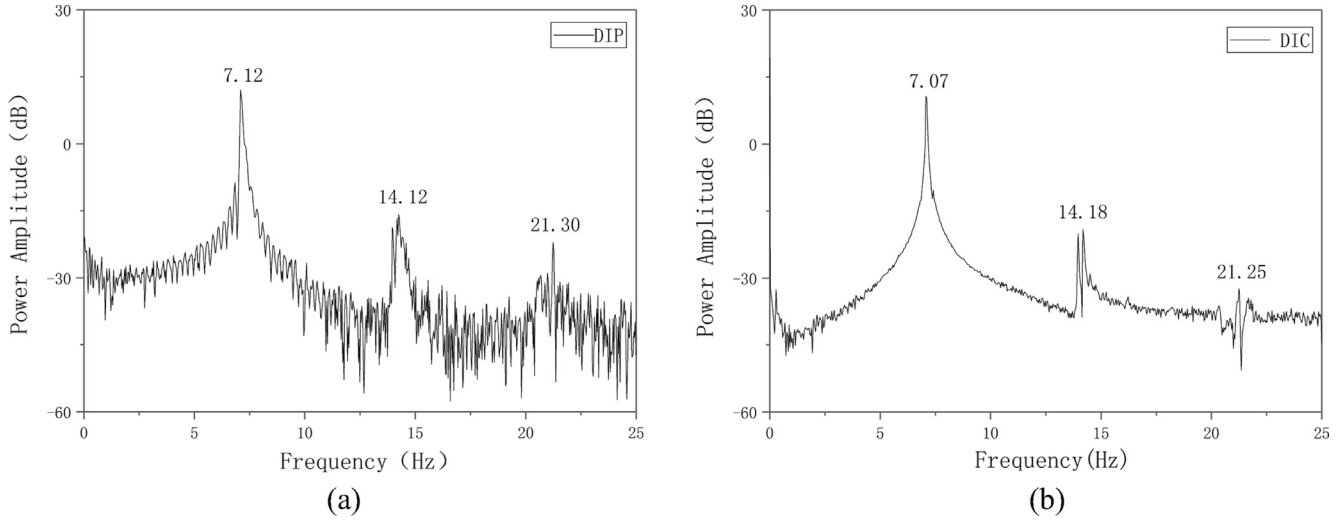

Fig. 7. (a) PSD function of stay cable R04 by digital image processing and (b) digital image correlation.

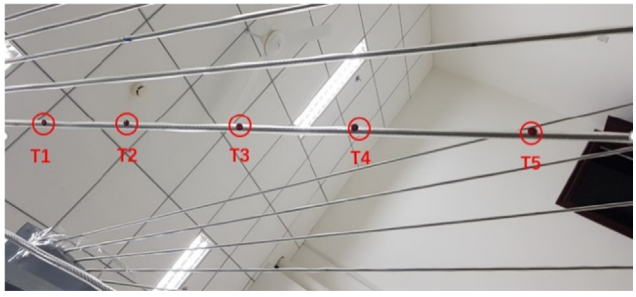

Fig.8. Five targets placement.

changes in light and the emergence of other dynamic backgrounds should be taken into account in practical engineering applications. More obvious targets such as LED lights could be arranged for easier identification to reduce the impact of light changes or bad weather. For the change of dynamic backgrounds, the selection of region of interest could be narrowed to get better processing results.

4. Conclusions

In this study, two kinds of digital image techniques were used in stay cable force measurement from single to multi-target, which can meet the requirements of engineering. The minimum deviation of cable force measurement at a single point is 0.24% and the maximum is 2.69%. The cable force measurement deviation of the multi-point is about 3.05%. Compared with previous works such as the researches of Kim et al. (the cable force deviation between digital image method and design value is about 5%) [14] and Feng et al. (the maximum discrepancy of vision sensor is 5.6% compared with load cell) [16], the results of this paper are famous. Comparatively speaking, DIP method shows better dynamic response performance.

The digital image techniques would be more reliable and convenient in bridge health monitoring, especially in cable force monitoring with the development of high-performance cameras. This paper presented the application of two digital image techniques in cable force monitoring, verified the reliability of the two methods with acceleration, and compared the differences between the two methods. The DIP method has the advantages of simple

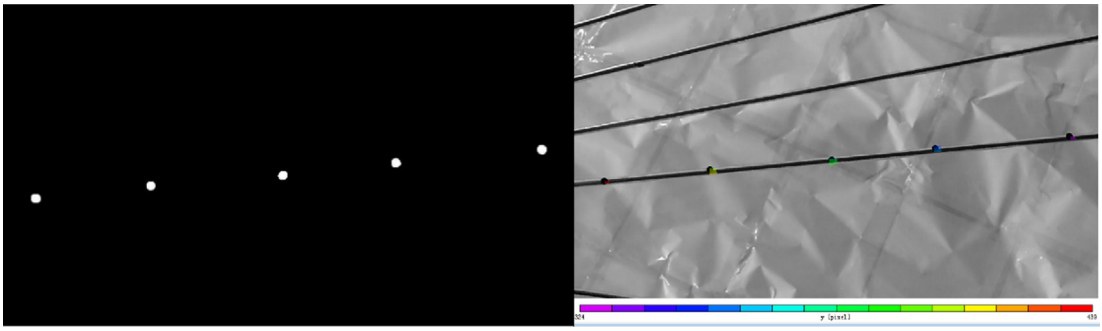

Fig. 9. Results of (a) digital image processing method and (b) digital image correlation method.

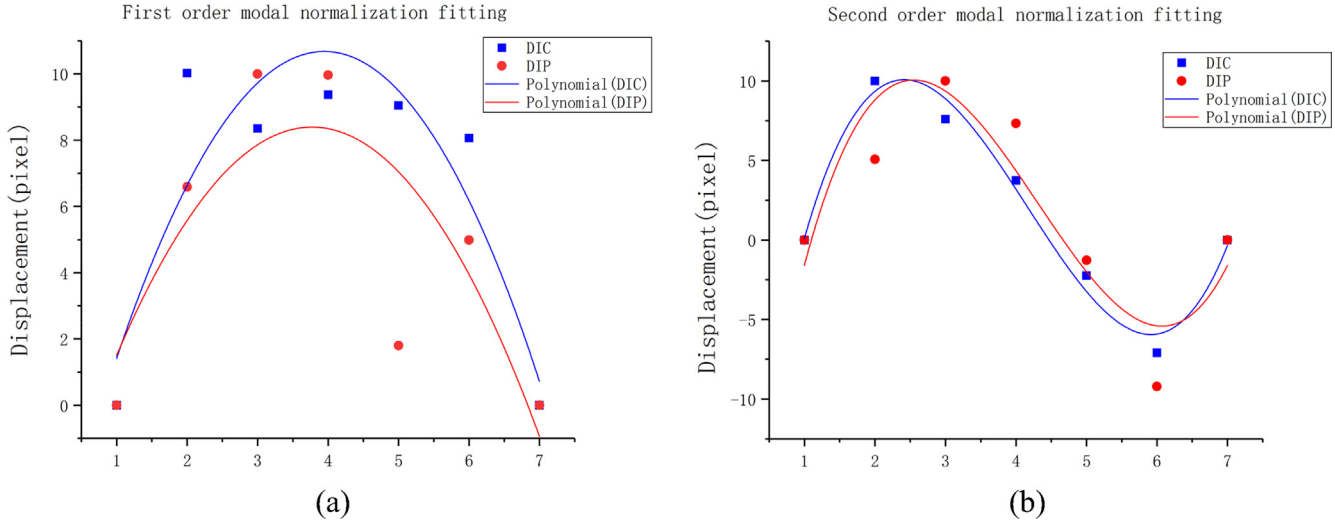

Fig. 10. (a) First and (b) second order modal analysis results of stay cable R08.

algorithm, convenient calculation and so on. The DIC method algorithm is relatively complex, but it has certain superiority for the feature recognition under the complex background. In the future monitoring process, different methods should be selected considering the characteristics of the two methods and the requirements of the actual project. DIP and DIC can also be used simultaneously for comparative analysis to increase the accuracy of cable force measurement. For digital image techniques, multi-target hunting is able to conclude mode information of stay cable and modify the outcome of single target to some extent. For these reasons, application of digital image techniques in bridge health monitoring will develop rapidly with the continuous improvement of technology.

It should be noted that despite the satisfactory results of the digital image techniques, several predictable problems during engineering application are still need to be tackled with in future studies, such as whether the lab test results are consistent with the actual bridge monitoring. These problems would be explored further in future studies and would be considered as a long-term study.

Declaration of Competing Interest

The authors declare that they have no known competing financial interests or personal relationships that could have appeared to influence the work reported in this paper.

Acknowledgements

This work is supported by the Fundamental Research Funds for the Central Universities [grant No. 2018B16814]; and National Natural Science Foundation of China [grant Nos. U1765204, 51679078].

References

[1] H. Zui, T. Shinke, Y. Namita, Practical formula for estimation of cable tension by vibration method, ASCE J. Struct. Eng. 122 (6) (1996) 651–656. http://refhub.elsevier.com/S0963-8695(13)00080-7/sbref6.
[2] T. Shimada, A Study on the Maintenance and Management of the Tension Measurement for the Cable of Bridge, Kobe University, 1995 (Ph dissertation).
[3] Wu. Wen-hwa, Chien-Chou Chen, Yu-Chuan Chen, et al., Tension determination for suspenders of arch bridge based on multiple vibration measurements concentrated at one end, Measurement 123 (March) (2018) 254–269, https://doi.org/10.1016/j.measurement.2018.03.077.
[4] C.-C. Chen, W.-H. Wu, M.-R. Leu, et al., Tension determination of stay cable or external tendon with complicated constraints using multiple vibration measurements, Measurement 86 (2016) 182–195, https://doi.org/10.1016/j.measurement.2016.02.053.
[5] Z. Chen, H. Li, Y. Bao, N. Li, Y. Jin, Identification of spatio-temporal distribution of vehicle loads on long-span bridges using computer vision technology, Struct. Control Health Monit. 23 (3) (2016) 517–534, https://doi.org/10.1002/stc.1780.
[6] Billie F. Spencer, Vedhus Hoskere, Yasutaka Narazaki, Advances in computer vision-based civil infrastructure inspection and monitoring, Engineering 5 (2) (2019) 199–222, https://doi.org/10.1016/j.eng.2018.11.030.
[7] R.P. Bigger, A. Carpenter, N. Scott, et al., Dynamic response of aluminum 5083 during Taylor impact using digital image correlation, Exp. Mech. 58 (6) (2018) 951–961, https://doi.org/10.1007/s11340-018-0392-5.

[8] Ho-Hoai Nam, Ki Deok Kim, Young Soo Park, Jong Jae Lee, An efficient image-based damage detection for cable surface in cable-stayed bridges, NDT E Int. 58 (2013) 18–23, https://doi.org/10.1016/j.ndteint.2013.04.006.
[9] M. Mahal, T. Blanksvärd, B. Täljsten, et al., Using digital image correlation to evaluate fatigue behavior of strengthened reinforced concrete beams, Eng. Struct. 105 (2015) 277–288, https://doi.org/10.1016/j.engstruct.2015.10.017.
[10] C.C. Chang, Y.F. Ji, Flexible videogrammetric technique for three-dimensional structural vibration, Measurement 133 (2007) 656–664, https://doi.org/10.1061/(ASCE)0733-9399(2007)133:6(656).
[11] J.J. Lee, M. Shinozuka, Real-time displacement measurement of a flexible bridge using digital image processing techniques, Exp. Mech. 46 (2006) 105–114, https://doi.org/10.1007/s11340-006-6124-2.
[12] H.S. Choi, J.H. Cheung, S.H. Kim, et al., Structural dynamic displacement vision system using digital image processing, NDT E Int. 44 (2011) 597–608, https://doi.org/10.1007/s11340-006-6124-2.
[13] Kim Sung-wan, Nam-sik Kim, Dynamic characteristics of suspension bridge hanger cables using digital image processing, NDT E Int. 59 (2013) 25–33, https://doi.org/10.1016/j.ndteint.2013.05.002.
[14] Kim Sung-wan, Bub-gyu Jeon, Nam-sik Kim, et al., Vision-based monitoring system for evaluating cable tensile forces on a cable-stayed bridge, Struct. Healthy Monitor. 12 (5–6) (2013) 440–456, https://doi.org/10.1177/1475921713500513.
[15] L. Tian, B. Pan, Remote bridge deflection measurement using an advanced video deflectometer and actively illuminated LED targets, Sensors (Basel, Switzerland). 16 (2016) 1344, https://doi.org/10.3390/s16091344.
[16] D. Feng, T. Scarangello, M.Q. Feng, et al., Cable tension force estimate using novel noncontact vision-based sensor, Measurement 99 (2017) 44–52, https://doi.org/10.1016/j.measurement.2016.12.020.
[17] Xinke Li, Chao Gao, Yongcai Guo, et al., Cable surface damage detection in cable-stayed bridges using optical techniques and image mosaicking, Opt. Laser Technol. 110 (2019) 36–43, https://doi.org/10.1016/j.optlastec.2018.07.012.
[18] A. Ellenberg, L. Branco, A. Krick, et al., Use of unmanned aerial vehicle for quantitative infrastructure evaluation, J. Infrastruct. Syst. 21 (3) (2014) 04014054, https://doi.org/10.1061/(ASCE)IS.1943-555X.0000246.
[19] G. Morgenthal, N. Hallermann, Quality assessment of unmanned aerial vehicle (UAV) based visual inspection of structures, Adv. Struct. Eng. 17 (3) (2014) 289–302, https://doi.org/10.1260/1369-4332.17.3.289.
[20] S. Rathinam, Z.W. Kim, R. Sengupta, Vision-based monitoring of locally linear structures using an unmanned aerial vehicle, J. Infrastruct. Syst. 14 (1) (2008) 52–63, https://doi.org/10.1061/(ASCE)1076-0342(2008)14:1(52).
[21] T. Omar, M.L. Nehdi, Remote sensing of concrete bridge decks using unmanned aerial vehicle infrared thermography, Autom. Constr. 83 (Nov) (2017) 360–371, https://doi.org/10.1016/j.autcon.2017.06.024.
[22] F.C. Pereira, C.E. Pereira, Embedded image processing systems for automatic recognition of cracks using UAVs, IFAC-Papers OnLine 48 (10) (2017) 16–21, https://doi.org/10.1016/j.ifacol.2015.08.101.
[23] Bin Lei, Ning Wang, Xu. Pengcheng, et al., New crack detection method for bridge inspection using UAV incorporating image processing, J. Aerosp. Eng. 31 (5) (2018) 04018058, https://doi.org/10.1061/(ASCE)AS.1943-5525.0000879.
[24] Daniel Reagan, Alessandro Sabato, Christopher Niezrecki, Feasibility of using digital image correlation for unmanned aerial vehicle structural health monitoring of bridges, Struct. Health Monitor. 17 (5) (2018), https://doi.org/10.1177/1475921717735326.
[25] R. Hang, P. Isola, A.A. Efros, Split-brain autoencoders: unsupervised learning by cross-channel prediction, in: Proceedings of 2017 IEEE Conference on Computer Vision and Pattern Recognition; 2017 Jul 21–26; Honolulu, HI, USA, IEEE, Piscataway, 2017, pp. 645–654.
[26] L. Zhang, F. Yang, Y.D. Zhang, et al., Road crack detection using deep convolutional neural network, in: Proceedings of 2016 IEEE International Conference on Image Processing; 2016 Sep 25–28; Phoenix, AZ, USA, IEEE, Piscataway, 2016, pp. 3708–3712, https://doi.org/10.1109/ICIP.2016.7533052.
[27] Zhentian Huang, Dong Lei, Yuan Wang, Modified moving least square collocation method for solving wave equations, Adv. Appl. Math. Mech. 10 (2019) 1–17, https://doi.org/10.4208/aamm.OA-2018-0029.
[28] Y.J. Cha, W. Choi, O. Büyüköztürk, Deep learning-based crack damage detection using convolution alneural networks, Comput.-Aided Civ. Infrastruct. Eng. 32 (5) (2017) 361–378, https://doi.org/10.1111/mice.12263.
[29] Y. Gao, K.M. Mosalam, Deep transfer learning for image-based structural damage recognition, Comput.-Aided Civ. Infrastruct. Eng. 33 (9) (2018) 748–768. https://www2.scopus.com/sourceid/18144?origin=recordpage.
[30] Billie F. Spencer Jr., Vedhus Hoskere, Yasutaka Narazaki, Advances in computer vision-based civil infrastructure inspection and monitoring, Engineering 5 (2019) 199–222, https://doi.org/10.1016/j.eng.2018.11.030.
[31] D. Feng, M.Q. Feng, Computer vision for SHM of civil infrastructure: from dynamic response measurement to damage detection – a review, Eng. Struct. 156 (2018) 105–117, https://doi.org/10.1016/j.engstruct.2017.11.018.
[32] B. Pan, L. Tian, X. Song, Real-time, non-contact and targetless measurement of vertical deflection of bridges using off-axis digital image correlation, NDT E Int. 79 (2016) 73–80, https://doi.org/10.1016/j.ndteint.2015.12.006.
[33] M.N. Helfrick, C. Niezrecki, P. Avitabile, et al., 3D digital image correlation methods for full-field vibration measurement, Mech. Syst. Sig. Process. 25 (3) (2011) 917–927, https://doi.org/10.1016/j.ymssp.2010.08.013.
[34] D. Mas, B. Ferrer, P. Acevedo, et al., Methods and algorithms for video-based multi-point frequency measuring and mapping, Measurement 85 (2016) 164–174, https://doi.org/10.1016/j.measurement.2016.02.042-40.
[35] M.A. Sutton, F. Matta, D. Rizos, et al., Recent progress in digital image correlation: background and developments since the 2013 W M Murray lecture, Exp. Mech. 57 (1) (2017) 1–30, https://doi.org/10.1007/s11340-016-0233-3.
[36] B. Pan, Digital image correlation for surface deformation measurement: historical developments, recent advances and future goals, Meas. Sci. Technol. 29 (8) (2018), https://doi.org/10.1088/1361-6501/aac55b 082001.
[37] Dong Lei, Zhentian Huang, Pengxiang Bai, et al., Experimental research on impact damage of Xiaowan arch dam model by digital image correlation, Constr. Build. Mater. 147 (2017) 168–173, https://doi.org/10.1016/j.conbuildmat.2017.04.143.
[38] Feipeng Zhu, Pengxiang Bai, Yan Gong, et al., Accurate measurement of elastic modulus of specimen with initial bending using two-dimensional DIC and dual-reflector imaging technique, Measurement 119 (2018) 18–27, https://doi.org/10.1016/j.measurement.2018.01.043.
[39] B.N. Zhao, D. Lei, J.J. Fu, et al., Experimental study on micro-damage identification in reinforced concrete beam with wavelet packet and DIC method, Constr. Build. Mater. 210 (2019) 338–346, https://doi.org/10.1016/j.conbuildmat.2019.03.175.
[40] F. Zhu, R. Lu, P. Bai, et al., A novel in situ calibration of object distance of an imaging lens based on optical refraction and two-dimensional DIC, Opt. Lasers Eng. 120 (2019) 110–117, https://doi.org/10.1016/j.optlaseng.2019.03.023.
[41] R. Ghorbani, F. Matta, M.A. Sutton, Full-field deformation measurement and crack mapping on confined masonry walls using digital image correlation, Exp. Mech. 55 (1) (2015) 227–243, https://doi.org/10.1002/stc.1780.
[42] J.P. Lewis, Fast normalized cross-correlation. Research Gate, 2013. https://www.researchgate.net/publication/2378357.
[43] Zhentian Huang, Dong Lei, Zi Han, Pei Zhang, Boundary moving least square method for numerical evaluation of two-dimensional elastic membrane and plate dynamics problems, Eng. Anal. Boundary Elem. 108 (2019) 41–48, https://doi.org/10.1016/j.enganabound.2019.08.002.